Nanopatterning self-assembled nanoparticle superlattices by moulding microdroplets

WENLONG CHENG, NOKYOUNG PARK, M. TODD WALTER, MARK R. HARTMAN AND DAN LUO*

Department of Biological & Environmental Engineering, Cornell University, Ithaca, New York 14853, USA
***e-mail: dan.luo@cornell.edu**

Published online: 28 September 2008; doi:10.1038/nnano.2008.279

Highly ordered arrays of nanoparticles exhibit many properties that are not found in their disordered counterparts. However, these nanoparticle superlattices usually form in a far-from-equilibrium dewetting process, which precludes the use of conventional patterning methods owing to a lack of control over the local dewetting dynamics. Here, we report a simple yet efficient approach for patterning such superlattices that involves moulding microdroplets containing the nanoparticles and spatially regulating their dewetting process. This approach can provide rational control over the local nucleation and growth of the nanoparticle superlattices. Using DNA-capped gold nanoparticles as a model system, we have patterned nanoparticle superlattices over large areas into a number of versatile structures with high degrees of internal order, including single-particle-width corrals, single-particle-thickness microdiscs and submicrometre-sized 'supra-crystals'. Remarkably, these features could be addressed by micropatterned electrode arrays, suggesting potential applications in bottom-up nanodevices.

The development of parallel, inexpensive approaches to patterning crystalline materials is essential in making use of their outstanding properties in bottom-up nanodevices[1,2]. Nanoparticle superlattices comprise a new class of crystals ('supra-crystal') with collective properties that are different from those of bulk phase materials, isolated nanoparticles and even disordered nanoparticle assemblies[3–11]. For instance, coherent vibrational modes can only appear in highly ordered nanoparticle superlattices[12], and synergistic effects in superlattices can lead to enhanced p-type conductivity[13]. Hence, nanoparticle superlattices are poised to become a 'new periodic table'[14], which could be used for high-performance devices such as high-density data storage, more efficient energy harvesting systems and ultra-sensitive biosensors.

Applying the collective properties of nanoparticle superlattice entities in nanodevices usually requires methods capable of patterning them into desired structures while maintaining a high degree of internal order. However, superlattices usually form from the evaporation of a drop of nanoparticle solution, which is essentially a far-from-equilibrium process[3–11]. Capillary flow induced by a non-uniform evaporation field[15] and fluid fluctuations during late-stage drying[16] often lead to irregular features such as isolated islands, worm-like domains, ring-like structures and cellular networks[17,18]. Owing to the statistical nature of drying-mediated self-assembly, it remains a challenge to pattern superlattices with comprehensive control over internal order and overall morphologies. Recently, several experimental techniques have been developed to pattern nanoparticles, but these efforts have not attained a high degree of internal order owing to a lack of control over local dewetting dynamics[17–23]. Conceivably, these limitations can be overcome by generating patterned microdroplets containing nanoparticles and locally controlling the nucleation and growth of superlattices. Chemically patterned surfaces[24–28] and the protrusions of stamps[29] have been used to generate patterned liquid microdroplets. However, shapes and contact line boundaries of individual microdroplets cannot be precisely defined, resulting in unexpected microdroplet shapes and structural instabilities[25–27]. In addition, it remains unclear whether these approaches can be used for patterning nanoparticles.

Here, we present a conceptually new, simple and efficient nanoparticle superlattice-patterning method. By sandwiching a nanoparticle solution between a micropatterned polydimethylsiloxane (PDMS) mould and a solid substrate (see Supplementary Information, Fig. S1), we obtained 'moulded microdroplets' with precisely defined shapes, locations and contact line boundaries. We demonstrated that their local dewetting dynamics can be controlled by moulding pressures (sandwiching force applied to the top of the PDMS mould) and mould geometry. As a result, the local crystallization events were rationally regulated, leading to large-area patterned superlattices with a high degree of internal order. Using micrometre-sized moulds, we have achieved versatile nanoscale features, such as single-particle-width corrals (1D), single-particle-thickness microdiscs (2D), submicrometre-sized 'supra-crystals' (3D) and double corrals. Moreover, these patterned superlattices can be addressed by micropatterned electrode arrays. In addition, we further show that our approach can be generalized to other self-assembled crystalline materials. Notably, these results have not been achieved by existing patterning techniques, such as micromoulding (limited to viscous solutions[30,31] or open channels[30,32,33]) or edge lithography (restricted to disordered systems[20]). In contrast, our strategy provides spatial control over microdroplet shapes and dewetting, and most importantly, local crystallization. Hence, our approach constitutes a promising step towards integrating nanoparticle superlattices and other

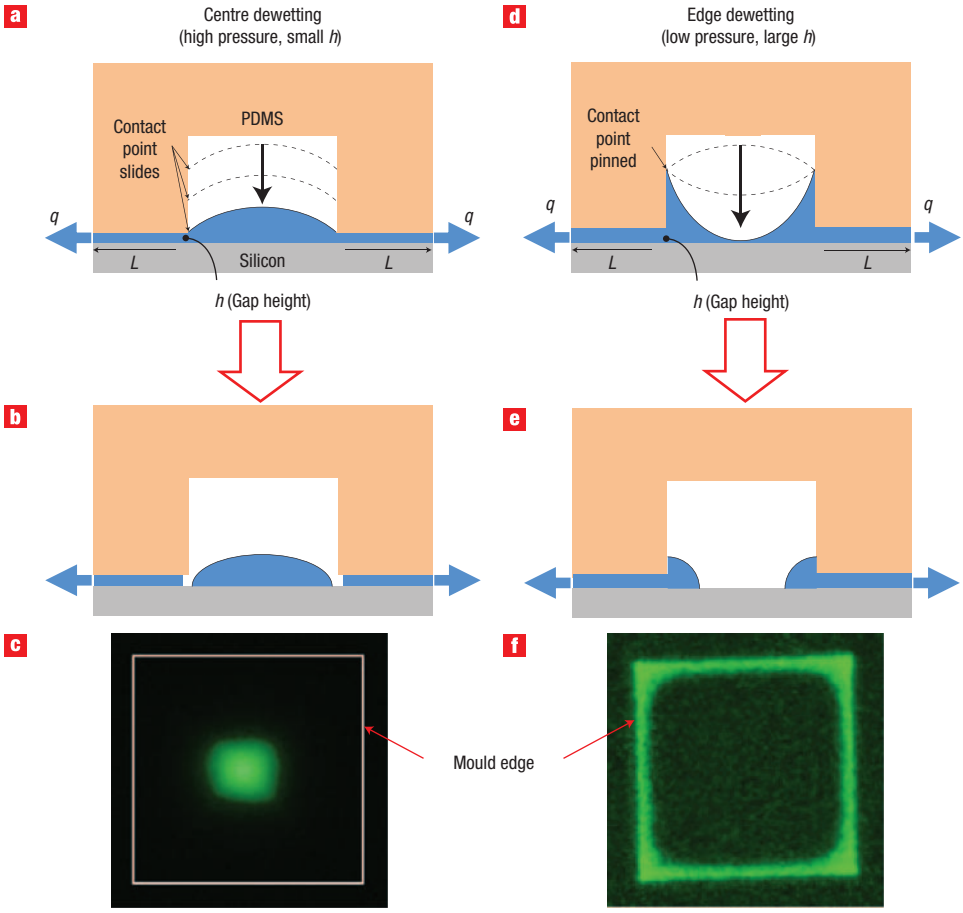

Figure 1 Cross-sectional schematic of a microdroplet confined in a micromould showing centre dewetting (a–c) and edge dewetting (d–f). Under high pressure the contact point between the microdroplet and micromould edge slips down the side of the micromould (**a**) and eventually breaks near the micromould edge, creating a microdroplet on the silicon substrate in the centre of the micromould (**b**). **c**, Fluorescent image of a microdroplet in the middle of a square micromould in a centre dewetting process. Under low pressure the contact point between the microdroplet and micromould remains pinned to the side of the micromould (**d**) and eventually breaks near the micromould middle, creating a microdroplet on the silicon substrate at the edge of the micromould (**e**). **f**, A fluorescent image of a microdroplet-corral formed at the edge of a square micromould in an edge dewetting process. Note that the initial shape of the meniscus within the micromould is consistent with observations of microdroplets in microwells[44].

drying-mediated crystalline materials into large-area electronic nanodevices.

MOULDING MICRODROPLETS AND REGULATING DEWETTING

Unlike natural water droplets, which usually have quasi-spherical cap shapes[34], moulded microdroplets can have well-defined shapes, volumes, locations and contact line boundaries (see Supplementary Information, Fig. S2). Under different pressures, these 'artificial' microdroplets display distinct, highly controllable dewetting dynamics (Fig. 1). When the mould is under high pressure, a single microdroplet forms on the substrate in the middle of a micromould (see Supplementary Information, Movie 1), a process we call 'centre dewetting'. For this to happen, the microdroplets must separate from the edges of the micromould. Conversely, under lower pressures we observe 'edge dewetting', during which the microdroplet collapses in the middle of the micromould, forming a 'microdroplet-corral' that remains attached to the edge of the micromould for some time (see Supplementary Information, Movie 2).

Based directly on dewetting observations, it is apparent that the solution–micromould contact point remains pinned during edge dewetting and slides down the micromould during centre dewetting. Although the three dimensional (3D) details of these processes are undoubtedly complex, our observations of edge and centre dewetting are consistent with recent research of solute drying from a moving meniscus[35]. Specifically, high solute concentrations at the air–solution–solid interface strengthen the forces pinning this contact point[15,36,37]. Others[35] have demonstrated that when the meniscus near the contact point deforms in a way that concentrates solutes near this point, the contact point will tend to remain pinned. Conversely, if the meniscus deforms in a way that keeps the area near the contact point diluted, the contact point will tend to slip. In our experiments, edge dewetting occurred very rapidly compared with centre dewetting. In centre dewetting, water was slowly drawn out of the bottom of the micromould, inducing a slow deformation of the meniscus. Under these conditions, internal currents within the solution are presumably sufficient to keep the solution near the contact point dilute and allow it to slip down the side of the micromould (Fig. 1a). Eventually, the contact point approaches the underlying substrate under the mould and breaks

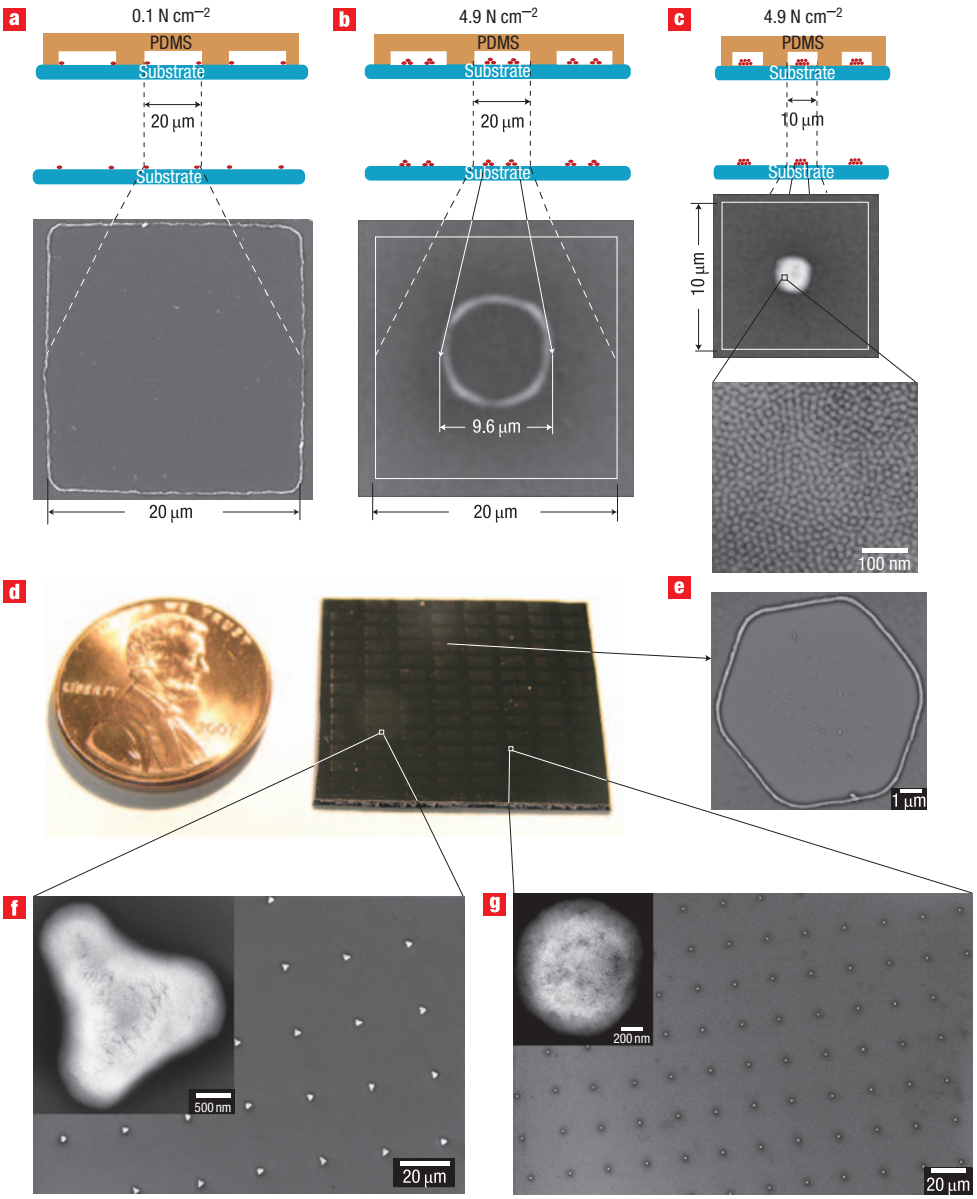

Figure 2 Patterning nanoparticle superlattices by means of local dewetting dynamics regulation. The nanoparticle concentration used was 400 nM. **a**, Edge-defined corrals obtained from a square micromould (side length = 20 μm, depth = 8.5 μm) in an edge dewetting process at a pressure of 0.1 N cm^{-2}. **b**, Shrunken nanoparticle micro-corral formed in a centre dewetting process using the same square micromould as in **a** but at a pressure of 4.9 N cm^{-2}. **c**, A 3D 'supra-crystal' formed in a centre dewetting process using a square micromould (side length = 10 μm, depth = 8.5 μm) at a pressure of 4.9 N cm^{-2}. **d**, Photograph of patterned superlattices on a silicon substrate. **e–g**, SEM micrographs of hexagonal nanoparticle corrals, triangle-like 'supra-crystals', and circular 'supra-crystals', respectively.

free of the micromould edge (Fig. 1b,c). Conversely, during edge dewetting the meniscus deforms rapidly, concentrating solutes at the edges and also enhancing evaporation near the edges, which further concentrates the solutes and helps pin the contact point to the micromould edge (Fig. 1d). The meniscus eventually ruptures in the centre when it approaches the substrate (Fig. 1e,f). To understand why the solution leaves the mould more slowly under high pressure (centre dewetting) than under low pressure (edge dewetting), consider Poiseuille's law for flow between parallel plates:

$$q = \frac{\Delta P h^4}{12 \mu L} \qquad (1)$$

where ΔP is the pressure gradient between the micromould and the edge of the mould, q is the flow out of the micromould, h is the gap height between the mould and the bottom substrate, μ is the dynamic viscosity of the solution, and L is the distance between the micromould and the edge of the mould (Fig. 1a). Because our mould 'floats' on the solute, ΔP and h are inversely related; thus, increased pressure decreases the gap height and has a large effect on retarding q, which explains why centre dewetting is slower than edge dewetting. Although we have only described situations of full contact point slip and pin, a variety of stick–slip behaviours may occur between these two conditions[35]. In addition, PDMS deformation may also influence meniscus shapes, leading to more complicated stick–slip motions.

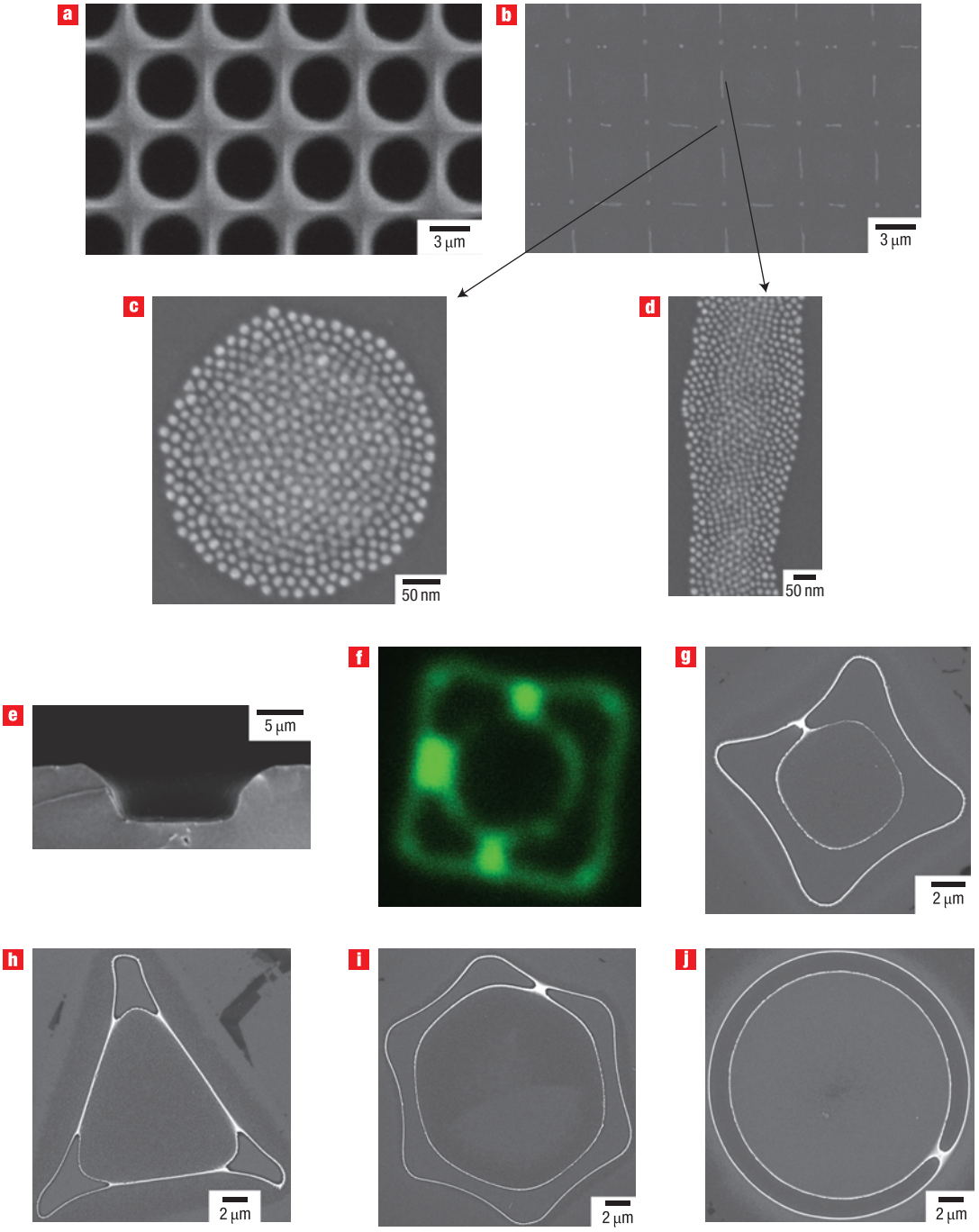

Figure 3 Versatile superlattice structures obtained by tailoring the inter-micromould spacing and micromould edge geometry. a, SEM micrograph of a PDMS mould with close-spaced features (see Methods for fabrication details). **b**, SEM micrograph of patterned superlattices on a silicon substrate using the close-spaced micromoulds. **c**,**d**, Magnified views of nanodiscs and nanolines, respectively, in **b. e**, Cross-sectional SEM micrograph of a PDMS micromould with blunt edge (see Methods for fabrication details). **f**, Fluorescent image of a drying water microdroplet containing AlexaFluor 488 in a square micromould with blunt edge. **g**–**j**, SEM micrographs of double-corral structures of superlattices formed in a blunt-edged square, triangular, hexagonal and circular micromould, respectively.

PATTERNING NANOPARTICLE SUPERLATTICES

Control over the dewetting dynamics of moulded microdroplets makes it possible to pattern a variety of materials through regulating local drying-mediated deposition of solutes on a surface. We used this method to pattern our recently developed, high-quality nanoparticle superlattices onto a silicon substrate. These superlattices formed from single-stranded DNA-capped gold nanoparticles in a drying-mediated self-assembly process (see Supplementary Information, Fig. S3). DNA was used here as a spacer ligand similar to alkyl ligands[3–8,10], unlike DNA-programmable self-assembly in buffer solutions[38,39]. DNA packing density and length are dominant factors determining the formation of high-quality superlattices and interparticle spacing.

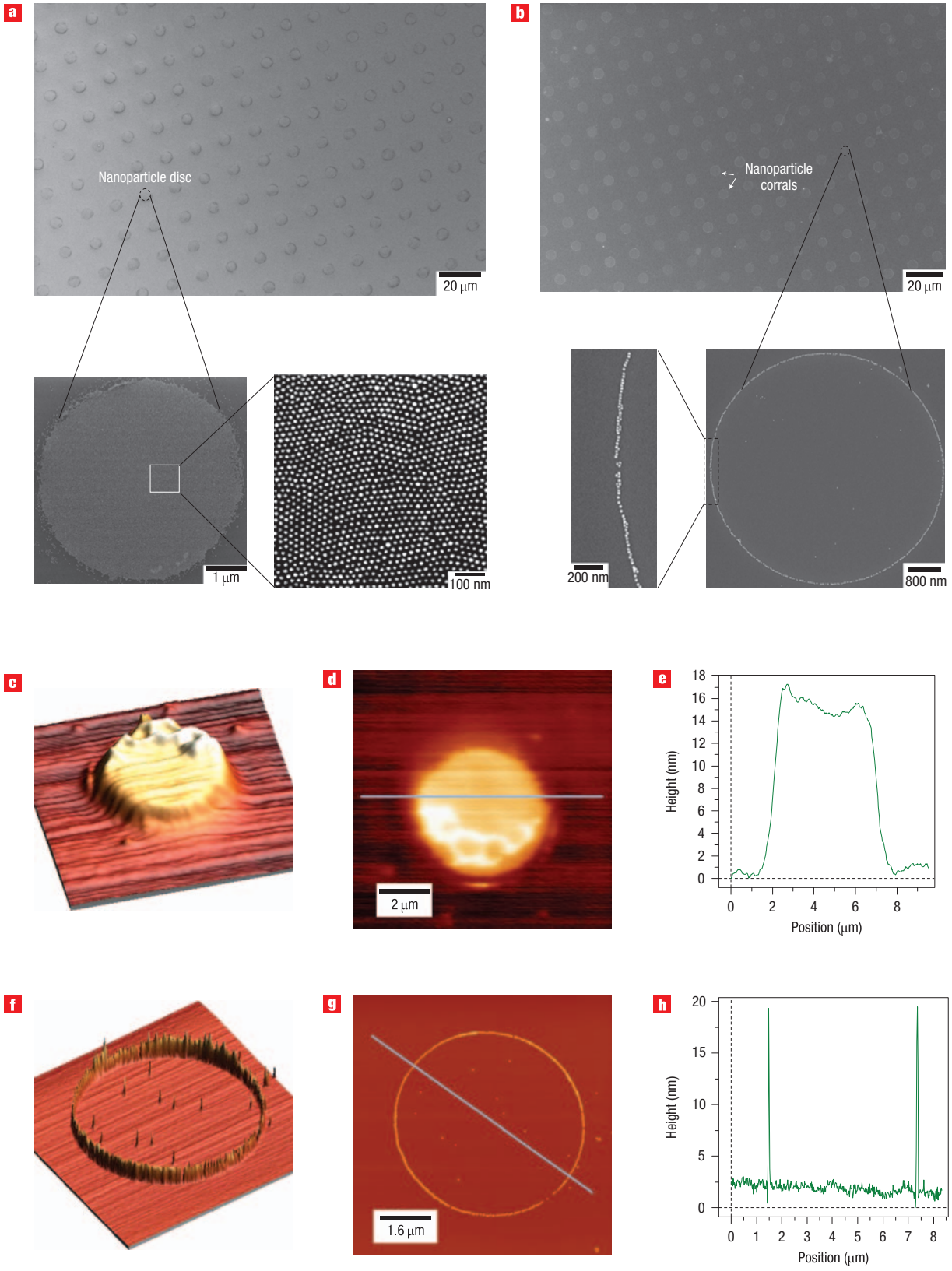

Figure 4 Monolayered superlattice microdiscs and single-particle-width micro-corrals. RIE-etched circular micromoulds (diameter = 5.0 μm, depth = 3.3 μm) were used. **a**, SEM micrographs of patterned microdiscs at different magnifications. The diffused edge observed might be due to adhesion of nanoparticles to the PDMS edge. Concentration of nanoparticles, 1.0 μM; moulding pressure, 3.0 N cm^{-2}. **b**, SEM micrographs of patterned single-particle-width micro-corrals. Concentration of nanoparticles, 330 nM; moulding pressure, 3.0 N cm^{-2}. **c**–**e**, AFM characterizations of a microdisc: 3D view (**c**); 2D view (**d**); surface plot of the corresponding line in **d** (**e**). **f**–**h**, AFM characterizations of a single-particle-width micro-corral: 3D view (**f**); 2D view (**g**); surface plot of the corresponding line in **g** (**h**).

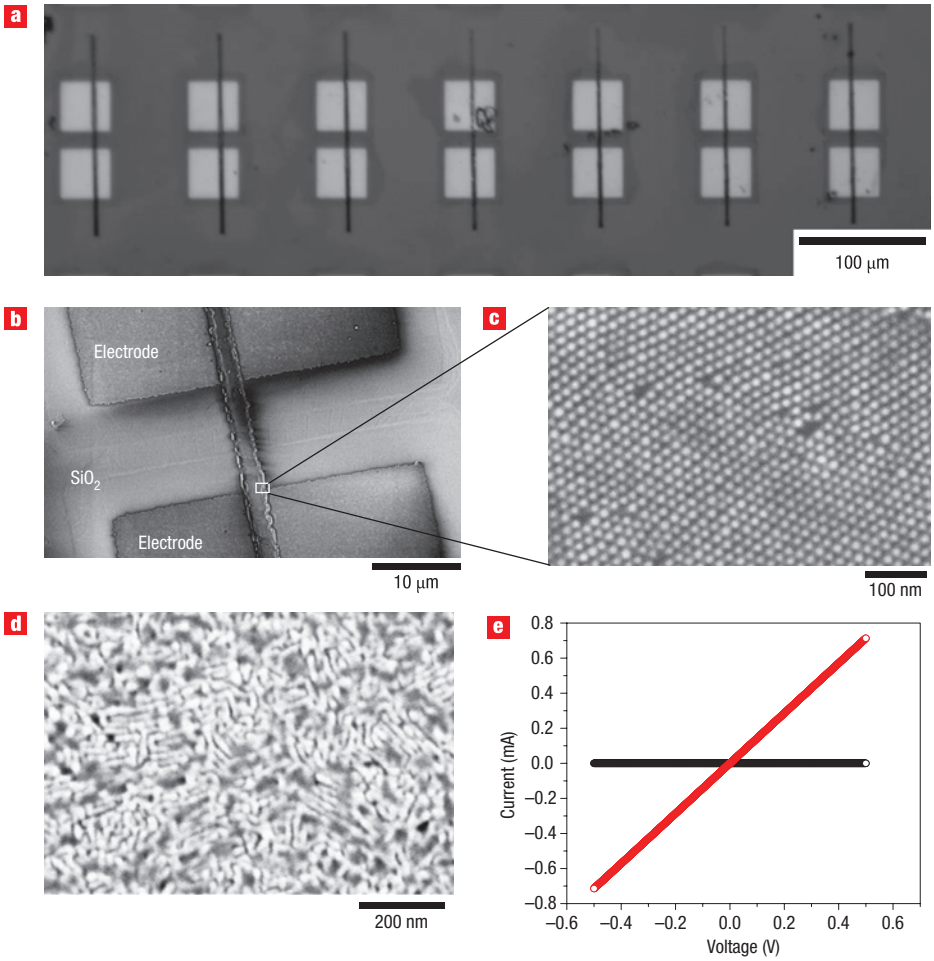

Figure 5 Addressing superlattices by micropatterned electrode arrays. a, Photograph of wires of monolayered superlattices across electrode pads. **b**,**c** SEM micrographs of a monolayered superlattice-bridged microelectrode pair. **d**, Fusion of nanoparticles into porous structures after annealing. **e**, *I*–*V* curve of a superlattice wire before (black circles) and after annealing (red circles) at 200 °C. The sequence of DNA is 5′-thiol-poly(dT)$_{15}$; concentration of nanoparticles, 800 nM; micromould depth, 5.3 μm; micromould width, 5.0 μm; moulding pressure, 2.0 N cm^{-2}.

The unique attributes of our superlattices are as follows: (i) DNA-capped nanoparticles have a high solubility in water (free of aggregation at an unusually high concentration of 83 mg ml^{-1}), enabling the patterning of 3D superlattices; (ii) the superlattices used here are in the size range of interesting surface plasmon resonance properties and can be readily imaged by scanning electron microscopy (SEM). By controlling local crystallization events of these DNA-capped gold nanoparticles using our approach, we have patterned superlattices into versatile features and investigated how moulding pressures, micromould geometry and particle concentrations influence their formation.

Under low moulding pressure, edge dewetting occurred, in which nucleation and growth of superlattices were confined to the micromould edges resulting in edge-defined corrals (Fig. 2a). These corrals remained intact on the silicon surface after peeling off the PDMS mould because of the strong adhesion between the nanoparticles and the high-surface-energy silicon substrate. Under intermediate moulding pressure, we observed well-formed edge-defined corrals and depinned corrals on the same substrate as a result of competing centre and edge dewetting (see Supplementary Information, Fig. S4). Under high moulding pressure, only centre dewetting occurred, in which nucleation and growth of superlattices were confined to the centre of the micromould, forming either a shrunken micro-corral (Fig. 2b) or a 3D 'supra-crystal' (Fig. 2c). Note that the shrunken micro-corral is still square-like, resembling its micromould geometry, which indicates that it might evolve from the edge-defined corrals formed at the early-stage dewetting. This observation indicates that the depinning of a microdroplet depends on its contact line geometry. For depinning to occur, the surface tension of a moulded microdroplet, γ_d, must overcome the resistance force of the nanoparticle deposit, σ_f, which has a higher value in the corner due to a higher surface-to-volume ratio. The shrinking nanoparticle deposit sticks to the substrate forming a micro-corral when γ_d cannot overcome σ_f (Fig. 2b); otherwise it develops into a 'supra-crystal' (Fig. 2c) before completely drying.

We also investigated the influence of micromould aspect ratios (depth/diameter) on overall morphologies of superlattices. Under the same pressure, edge dewetting dominated for a low-aspect-ratio micromould, whereas centre dewetting dominated for a high-aspect-ratio micromould (see Supplementary Information, Table S1). Hence, both corrals and 'supra-crystals' were obtained when micromoulds with different lateral dimensions were integrated into a single PDMS mould (Fig. 2d), allowing us to pattern superlattices into various structures on the same silicon substrate in a single step. Notably, our approach can be scaled to

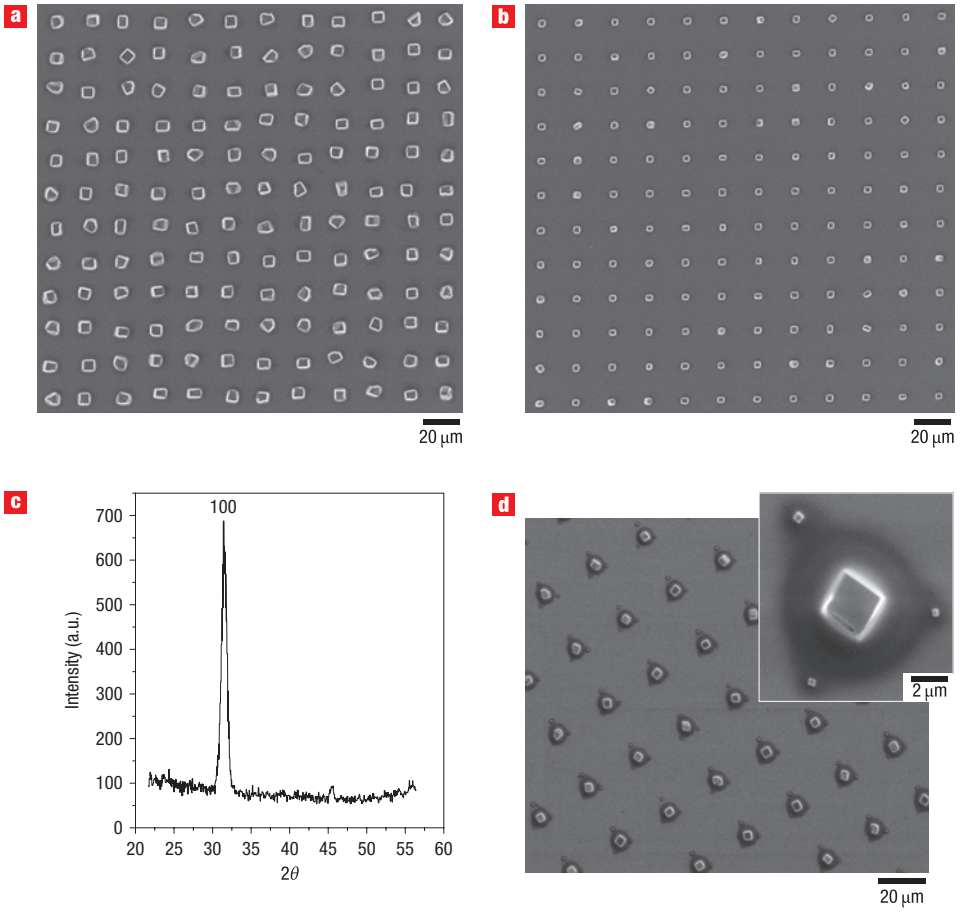

Figure 6 Patterning single-crystal arrays. a,**b**, SEM micrographs of patterned NaCl single-crystal arrays from square micromoulds. Concentration of NaCl, 2M; depth, 7.6 μm; moulding pressure, 3.1 N cm^{-2}. Micromould side length was 10 μm in **a** and 5 μm in **b**. **c**, X-ray diffraction pattern of NaCl single-crystal arrays in **a**. **d**, SEM micrograph of patterned NaCl single-crystal arrays from triangular micromoulds. Concentration of NaCl, 1 M; micromould side length, 20 μm, depth, 8.5 μm; moulding pressure, 1.4 N cm^{-2}.

pattern superlattices over a very large area. An image of patterned superlattices on a silicon substrate (20×25 mm^2) shows that the features are remarkably uniform given our unsophisticated means of pressure control (Fig. 2d–g).

We further explored the versatility of our nanopatterning methodology by investigating the influence of inter-micromould spacing and edge geometry on self-assembled superlattice structures. For close-spaced micromoulds (Fig. 3a; see Methods for fabrication details), neighbouring moulded microdroplets can merge during dewetting. In an edge dewetting process, microdroplets in neighbouring micromoulds formed dot-like and line-like microdroplets corresponding to the protrusions of micromould edges. As a result, the superlattices self-assembled into disc-like (Fig. 3c) and wire-like (Fig. 3d) assemblies with a high degree of internal order. In addition to spacing, edge geometry influenced local dewetting. For blunt-edged micromoulds (Fig. 3e; see Methods), larger depinning forces were required for microdroplets to separate than sharp-edged micromoulds, and, as a result, edge dewetting was favoured and thicker microdroplet-corrals were formed. In this situation, two discrete contact lines coexisted: an outer PDMS micromould edge-defined contact line and an inner contact line governed by surface tension. The water flow during dewetting was directed towards both pinned contact lines (Fig. 3f), leading to self-assembled superlattices with double-corral structures (Fig. 3 g–j). A high degree of internal order was well maintained in this self-assembly process (see Supplementary Information, Fig. S5). Interestingly, bridges formed between the inner and outer micro-corrals during the final stage of drying. Although these bridges were positioned randomly under current experimental conditions, defining their location might be possible if the spatial distribution of evaporation fluxes and water flow were directionally controlled.

In addition, we investigated the influence of concentration on superlattice features. For edge dewetting, as concentration increases, nanoparticle corrals become more continuous, with an increase in height and width (see Supplementary Information, Fig. S6). For centre dewetting, low concentration resulted in shrunken corrals, and high concentration allowed us to pattern 3D high-quality 'supra-crystals' (see Supplementary Information, Fig. S7).

To maintain a high degree of internal order, the nucleation and growth events of superlattices must be synchronized with the dewetting dynamics of moulded microdroplets. An important characteristic of DNA-capped gold nanoparticles is that the interparticle potential can be tuned by adjusting the salt concentration. If the salt concentration is too high, strong electrostatic screening assists rapid DNA hydrogen bonding, which locks nanoparticles together when they come into contact[40]. This rapid nucleation results in irreversible disordered aggregates at a low solubility limit. If the salt concentration is too

low, the interactions among nanoparticles are too repulsive for superlattices to nucleate and grow. In this situation, aggregation cannot occur until drying is nearly complete, which affords no annealing time for crystallization[40]. At a proper salt concentration (0.1–10 mM NaCl), we observed highly ordered superlattices. For sufficiently concentrated solutions, homogeneous nucleation occurred in moulded microdroplets, leading to patterned 'supra-crystals' (see Supplementary Information, Fig. S7). Otherwise, superlattices grew heterogeneously on the silicon substrate. When contact line crystallization was synchronized with centre and edge dewetting, we obtained monolayered nanoparticle microdiscs (Fig. 4a) and corrals (see Supplementary Information, Fig. S8), respectively. The width of nanoparticle micro-corrals could even be reduced to single-particle diameter (12 nm) (Fig. 4b, f–h), although some defects existed owing to the stochastic nature of drying-mediated self-assembly. Note that the 12-nm-width micro-corrals were obtained from 5-μm-diameter micromoulds, suggesting that our strategy constitutes a simple size reduction method. Compared with the template-confined organization of >100-nm polystyrene beads[33,41] or 60-nm nanoparticles[23], not only have we scaled particle size down to 12 nm, but we have also achieved single-particle-width features without using laborious high-resolution lithographic techniques such as electron beam lithography.

ADDRESSING SUPERLATTICES BY MICROPATTERNED ELECTRODES

As demonstrated above, moulding microdroplets is a straightforward and effective approach to patterning self-assembled superlattices on a surface. This combined top-down and bottom-up assembly strategy could ultimately impart unique properties of superlattices to future nanoscale optical and electronic devices. To realize such devices, a prerequisite will be the capability of constructing electrical interfacing of superlattices to microfabricated electrodes, which is illustrated here.

By sandwiching nanoparticle solutions between PDMS moulds and micropatterned electrode arrays with proper alignments, superlattices grew directly across microelectrodes (Fig. 5a,b). Despite the height difference between microelectrode pads and SiO_2 surfaces (60 nm), we demonstrated that superlattices were structurally continuous with a high degree of internal order (Fig. 5c). The average interparticle spacing was 20.6 ± 1.5 nm, corresponding to an edge-to-edge interparticle spacing of ~8 nm. Unlike close-spaced monolayer-protected-cluster films[42], the large gap in the monolayered superlattice prevented electron tunnelling from metal core to metal core, resulting in insulator-like electronic behaviour. The electronic properties of these unique superlattice wires can be further modulated by doping DNA-binding ions, dyes or superconductor molecules (such as Tetrathiafulvalene) or, more easily, by thermal annealing. For example, the nanoparticles fused and developed into porous metallic film after annealing (Fig. 5d), which enhanced electronic conductivities (Fig. 5e). A resistivity of $4.02 \times 10^{-7}\ \Omega$ m was obtained, which is ~16 times the bulk gold resistivity ($2.44 \times 10^{-8}\ \Omega$ m). The high resistivity is due to the porous nature of our nanoparticle wires. Hence, controlling porosity (for example, by programming the annealing temperature) will allow for tuning wire conductivities.

GENERALITY OF THE NANOPATTERNING APPROACH

The moulded microdroplet approach can be generalized to regulate the drying-mediated deposition of a variety of materials. We have demonstrated that it can be used to pattern CdSe/ZnS quantum dots and conducting polymers from dilute suspensions (see Supplementary Information, Figs S9 and S10) and it could, potentially, be used with organic solvents. Our preliminary attempts showed that high solvent volatility and PDMS swelling caused by non-polar solvent led to poor resolution of the resulting patterns. These limitations could be overcome through controlling the evaporation rate or by engineering the mould wetting properties.

Additionally, we demonstrated that our approach can be further extended to pattern single-crystal arrays. The most important parameters associated with crystallization—crystal size, nucleating location, density and crystallographic orientation—can be controlled through PDMS mould design and local dewetting regulation. SEM micrographs of patterned NaCl single-crystal arrays clearly show that we can precisely control crystal size and location (Fig. 6a,b). More interestingly, the orientations can also be controlled by micromould geometry. The cubic NaCl crystals grew with their facets parallel to the sides of square micromoulds owing to spatial confinement (Fig. 6a–c). X-ray characterization demonstrates that the top planes of these crystals are always (100) facets. For triangular micromoulds, cubic NaCl crystals did not match their corresponding mould geometries; in this case, four nucleating events occurred at the centre and three corners of each micromould (Fig. 6d). The corner nucleation is perhaps due to a longer retention time of the microdroplet at the corners, resulting from insufficient depinning forces. Remarkably, our approach can control local crystallization events in a single step with a high placement accuracy without any surface chemical treatment, as opposed to single-crystal patterning methods, which require surface modification[1,2].

Our results clearly show that drying-mediated crystallization of nanoparticle superlattices can be locally controlled by moulding microdroplets and regulating their dewetting dynamics. In addition to maintaining a high degree of order while patterning superlattices, we have also fabricated nanoscale features with dimensions far below those of the PDMS micromould. The superlattice entities can be addressed by micropatterned electrode arrays, which may ultimately result in application of their collective properties in practical optical and electronic nanodevices. In addition, we have demonstrated that our approach can be extended to patterning single-crystal arrays.

Although one of the unique advantages of our approach is the production of nanoscale features from micrometre-sized moulds, placement accuracy sometimes can be compromised by this size reduction process. We expect that the accuracy can be improved with a more sophisticated experimental setup. In addition, the PDMS mould deforms under pressure, which may complicate the dewetting process. In particular, PDMS can be further deformed by swelling in the presence of a non-polar organic solvent, which results in poor resolution. Nevertheless, rigid and solvent-resistant moulds can be used to improve resolutions, further extending our patterning approach to hydrophobic nanoparticles. We believe, therefore, that this generic method will lead to a quick and inexpensive route to patterning crystalline materials over a large area for exploring their outstanding properties in high-performance bottom-up devices.

METHODS

FABRICATION OF PDMS MOULDS

PDMS moulds were fabricated by moulding from a SU-8 master or reactive ion etching (RIE), depending on the specific requirements. The conventional PDMS moulds were prepared as follows. First, the SU-8 master was generated by standard photolithography followed by surface modification with trichloro(3,3,3-trifluoropropyl)silane. Then, a mixture of base and curing agent (10:1 w/w) of Sylgard 184 silicone elastomer was poured onto the patterned SU-8 surface and cured at 75 °C for 3 h. The PDMS moulds were obtained by peeling off from the SU-8 master.

To fabricate close-spaced or blunt-edged PDMS moulds, RIE was combined with photolithography. PDMS was first spin-coated onto O_2-plasma-treated

silicon wafers to a thickness of ~50 μm, followed by a layer of SPR 220-4.5 spin-coated to a thickness of 3–8 μm. In order to improve the adhesion, PDMS was treated with O_2 plasma before spin-coating the photoresist. After exposure and development, the patterned substrate was then dry etched using a 1:3 ratio of O_2:CF_4. The etch time was varied; short etch times resulted in a shallow micromould with sharp edges, and long etch times resulted in a deep micromould with smoothly curved (blunt) edges. For PDMS moulds with close-packed features, long etch times resulted in overlapping of neighbouring micromoulds.

MOULDING MICRODROPLETS AND PATTERN FORMATION

Both substrates and PDMS moulds were sonicated for 3 min in ethanol and dried before use. A droplet of aqueous solutions containing fluorescent dyes, nanoparticles, quantum dots, conducting polymers or salts was sandwiched between the PDMS mould and the solid substrate. A weight was placed on top of the PDMS mould to control the moulding pressure (see Supplementary Information, Fig. S1, for a typical setup). After complete drying of the microdroplets, the PDMS moulds were peeled off and deposits remained on the solid substrates.

SYNTHESIS OF DNA-CAPPED GOLD NANOPARTICLES

Gold nanoparticles with a diameter of ~12 nm were synthesized according to the literature[43]. ssDNA capped nanoparticles were synthesized according to ref. 38, with some modifications. 5′-Thiolated oligonucleotides (Integrated DNA Technologies) were deprotected and incubated with nanoparticle solutions at a 1,000:1 ratio of DNA to nanoparticle for 12 h at room temperature. Sodium chloride was then added to a final concentration of 0.2 M. The mixture was aged at room temperature for another 10–12 h. The mixture was centrifuged at 14,500 r.p.m. and the supernatant was exchanged with Milli-Q water.

INSTRUMENTATION

Transmission electron microscopy (TEM) images were acquired using a Tecnai T12 (FEI) operating at an acceleration voltage of 120 kV. Atomic force microscopy (AFM) measurements were carried out on a Dimension 3100 scanning probe microscope (Veeco Instruments) in tapping mode using a silicon cantilever. SEM images were obtained using a field-emission scanning electron microscope (ZEISS, LEO 1550) with an operating voltage of 2–5 kV. Microdroplets containing AlexaFluor 488 were imaged using a fluorescent microscope (Olympus, IX71). Conductivities were measured using the Agilent 4156C Precision Semiconducter Parameter Analyzer.

Received 10 June 2008; accepted 28 August 2008; published 28 September 2008.

References

1. Aizenberg, J., Black, A. J. & Whitesides, G. M. Control of crystal nucleation by patterned self-assembled monolayers. *Nature* **398,** 495–498 (1999).
2. Briseno, A. L. *et al.* Patterning organic single-crystal transistor arrays. *Nature* **444,** 913–917 (2006).
3. Murray, C. B., Kagan, C. R. & Bawendi, M. G. Self-organization of CdSe nanocrystallines into 3-dimensional quantum-dot superlattices. *Science* **270,** 1335–1338 (1995).
4. Kiely, C. J., Fink, J., Brust, M., Bethell, D. & Schiffrin, D. J. Spontaneous ordering of bimodal ensembles of nanoscopic gold clusters. *Nature* **396,** 444–446 (1998).
5. Pileni, M. P. Nanocrystal self-assemblies: Fabrication and collective properties. *J. Phys. Chem. B* **105,** 3358–3371 (2001).
6. Shevchenko, E. V., Talapin, D. V., Kotov, N. A., O'Brien, S. & Murray, C. B. Structural diversity in binary nanoparticle superlattices. *Nature* **439,** 55–59 (2006).
7. Kalsin, A. M. *et al.* Electrostatic self-assembly of binary nanoparticle crystals with a diamond-like lattice. *Science* **312,** 420–424 (2006).
8. Bigioni, T. P. *et al.* Kinetically driven self assembly of highly ordered nanoparticle monolayers. *Nature Mater.* **5,** 265–270 (2006).
9. Collier, C. P., Saykally, R. J., Shiang, J. J., Henrichs, S. E. & Heath, J. R. Reversible tuning of silver quantum dot monolayers through the metal–insulator transition. *Science* **277,** 1978–1981 (1997).
10. Korgel, B. A., Fullam, S., Connolly, S. & Fitzmaurice, D. Assembly and self-organization of silver nanocrystal superlattices: Ordered 'soft spheres'. *J. Phys. Chem. B* **102,** 8379–8388 (1998).
11. Mueggenburg, K. E., Lin, X. M., Goldsmith, R. H. & Jaeger, H. M. Elastic membranes of close-packed nanoparticle arrays. *Nature Mater.* **6,** 656–660 (2007).
12. Courty, A., Mermet, A., Albouy, P. A., Duval, E. & Pileni, M. P. Vibrational coherence of self-organized silver nanocrystals in f.c.c. supra-crystals. *Nature Mater.* **4,** 395–398 (2005).
13. Urban, J. J., Talapin, D. V., Shevchenko, E. V., Kagan, C. R. & Murray, C. B. Synergism in binary nanocrystal superlattices leads to enhanced p-type conductivity in self-assembled PbTe/Ag–2 Te thin films. *Nature Mater.* **6,** 115–121 (2007).
14. Shevchenko, E. V., Talapin, D. V., Murray, C. B. & O'Brien, S. Structural characterization of self-assembled multifunctional binary nanoparticle superlattices. *J. Am .Chem. Soc.* **128,** 3620–3637 (2006).
15. Deegan, R. D. *et al.* Capillary flow as the cause of ring stains from dried liquid drops. *Nature* **389,** 827–829 (1997).
16. Rabani, E., Reichman, D. R., Geissler, P. L. & Brus, L. E. Drying-mediated self-assembly of nanoparticles. *Nature* **426,** 271–274 (2003).
17. Martin, C. P. *et al.* Controlling pattern formation in nanoparticle assemblies via directed solvent dewetting. *Phys. Rev. Lett.* **99,** 116103 (2007).
18. Huang, J. X., Fan, R., Connor, S. & Yang, P. D. One-step patterning of aligned nanowire arrays by programmed dip coating. *Angew. Chem. Int. Ed.* **46,** 2414–2417 (2007).
19. Hamann, H. F., Woods, S. I. & Sun, S. H. Direct thermal patterning of self-assembled nanoparticles. *Nano Lett.* **3,** 1643–1645 (2003).
20. Cherniavskaya, O. *et al.* Edge transfer lithography of molecular and nanoparticle materials. *Langmuir* **18,** 7029–7034 (2002).
21. Lu, N. *et al.* Lateral patterning of luminescent CdSe nanocrystals by selective dewetting from self-assembled organic templates. *Nano Lett.* **4,** 885–888 (2004).
22. Santhanam, V. & Andres, R. P. Microcontact printing of uniform nanoparticle arrays. *Nano Lett.* **4,** 41–44 (2004).
23. Kraus, T. *et al.* Nanoparticle printing with single-particle resolution. *Nature Nanotech.* **2,** 570–576 (2007).
24. Kumar, A. & Whitesides, G. M. Patterned condensation figures as optical diffraction gratings. *Science* **263,** 60–62 (1994).
25. Gau, H., Herminghaus, S., Lenz, P. & Lipowsky, R. Liquid morphologies on structured surfaces: From microchannels to microchips. *Science* **283,** 46–49 (1999).
26. Lenz, P. & Lipowsky, R. Morphological transitions of wetting layers on structured surfaces. *Phys. Rev. Lett.* **80,** 1920–1923 (1998).
27. Lenz, P. Wetting phenomena on structured surfaces. *Adv. Mater.* **11,** 1531–1534 (1999).
28. Xia, Y. N., Qin, D. & Yin, Y. D. Surface patterning and its application in wetting/dewetting studies. *Curr. Opin. Colloid Interface Sci.* **6,** 54–64 (2001).
29. Cavallini, M. & Biscarini, F. Nanostructuring conjugated materials by lithographically controlled wetting. *Nano Lett.* **3,** 1269–1271 (2003).
30. Xia, Y. N. & Whitesides, G. M. Soft lithography. *Annu. Rev. Mater. Sci.* **28,** 153–184 (1998).
31. Klajn, R. *et al.* Plastic and mouldable metals by self-assembly of sticky nanoparticle aggregates. *Science* **316,** 261–264 (2007).
32. Kim, E., Xia, Y. N. & Whitesides, G. M. Two- and three-dimensional crystallization of polymeric microspheres by micromoulding in capillaries. *Adv. Mater.* **8,** 245–247 (1996).
33. Kim, E., Xia, Y. N. & Whitesides, G. M. Micromoulding in capillaries: Applications in materials science. *J. Am. Chem. Soc.* **118,** 5722–5731 (1996).
34. Dussan, E. B. Spreading of liquids on solid-surfaces—static and dynamic contact lines. *Annu. Rev. Fluid Mech.* **11,** 371–400 (1979).
35. Rio, E., Daerr, A., Lequeux, F. & Limat, L. Moving contact lines of a colloidal suspension in the presence of drying. *Langmuir* **22,** 3186–3191 (2006).
36. Deegan, R. D. *et al.* Contact line deposits in an evaporating drop. *Phys. Rev. E* **62,** 756–765 (2000).
37. Shmuylovich, L., Shen, A. Q. & Stone, H. A. Surface morphology of drying latex films: Multiple ring formation. *Langmuir* **18,** 3441–3445 (2002).
38. Mirkin, C. A., Letsinger, R. L., Mucic, R. C. & Storhoff, J. J. A DNA-based method for rationally assembling nanoparticles into macroscopic materials. *Nature* **382,** 607–609 (1996).
39. Alivisatos, A. P. *et al.* Organization of 'nanocrystal molecules' using DNA. *Nature* **382,** 609–611 (1996).
40. Velev, O. D. Self-assembly of unusual nanoparticle crystals. *Science* **312,** 376–377 (2006).
41. Yin, Y. D., Lu, Y., Gates, B. & Xia, Y. N. Template-assisted self-assembly: A practical route to complex aggregates of monodispersed colloids with well-defined sizes, shapes and structures. *J. Am. Chem. Soc.* **123,** 8718–8729 (2001).
42. Leopold, M. C. *et al.* Growth, conductivity and vapor response properties of metal ion–carboxylate linked nanoparticle films. *Faraday Discuss.* **125,** 63–76 (2004).
43. Frens, G. Controlled nucleation for regulation of particle-size in monodisperse gold suspensions. *Nature Phys. Sci.* **241,** 20–22 (1973).
44. Rieger, B., van den Doel, L. R. & van Vliet, L. J. Ring formation in nanolitre cups: Quantitative measurements of flow in micromachined wells. *Phys. Rev. E* **68,** 036312 (2003).

Supplementary Information accompanies this paper at www.nature.com/naturenanotechnology.

Acknowledgements

The authors thank J. Jung-Jen Li, J. Kahn, M. Campolongo, V. Pinskiy and V.L. Morales for technical help and discussions. The work is partially supported by NYSTAR and NSF CAREER award (grant number 0547330). The authors also thank J.C. March for proof-reading this manuscript. N.P. wishes to acknowledge the Korea Research Foundation Grant (04-03-05-2) for support.

Author contributions

W.L.C. and D.L. conceived and designed the experiments. W.L.C., N.P. and M.R.H. performed the experiments. W.L.C. and D.L. analysed the data. W.L.C., N.P., M.T.W., M.R.H. and D.L. co-wrote the paper. All authors discussed the results and commented on the manuscript.

Author information

Reprints and permission information is available online at http://npg.nature.com/reprintsandpermissions/. Correspondence and requests for materials should be addressed to D.L.